Heliyon 7 (2021) e07675

Contents lists available at ScienceDirect

Heliyon

journal homepage: www.cell.com/heliyon

Research article

Deposition of low-density thick silica films from burning sol-gel derived alcogels

Martin Timusk [a,*], Triin Kangur [a], Meeri Visnapuu [a], Siim Pikker [a], Andris Šutka [a,b], Martin Järvekülg [a]

[a] Institute of Physics, University of Tartu, W. Ostwaldi Str. 1, 50411 Tartu, Estonia
[b] Research Laboratory of Functional Materials Technologies, Faculty of Materials Science and Applied Chemistry, Riga Technical University, Paula Valdena 3/7, 1048 Riga, Latvia

ARTICLE INFO

Keywords:
Porous silica
Low density
Silanol-free
Sol-gel
Combustion synthesis

ABSTRACT

In the current study we show that the combustion of sol-gel derived alcogels with specifically tailored composition leads to the release of silica nanoparticles from the burning alcogel in a controlled manner which enables direct deposition of the released nanoparticles into low-density silica thick films. The process has some similarities to flame spray pyrolysis but requires no aerosol generator or other sophisticated instrumental setup. By the proper choice of catalysts and mixture of silicon alkoxides for the synthesis of the alcogel, preferential hydrolysis and polycondensation of one of the alkoxides is achieved. This leads to the formation of an alcogel with volatile silica precursor trapped in the gel pores. Resulting alcogels were burned to deposit uniform porous silica films with density of ~0.1 g/cm^3 and primary particle size of ~10 nm. Demonstrated method yields silanol-free silica directly, without additional treatment steps and enables straightforward control over the deposition rate and coarseness of the layer by simple adjustment of the composition of the silica alcogel. The maximum layer thickness is limited only by the deposition time (in the current work up to 134 μm). Such technique of porous oxide film preparation could potentially be extended to the preparation of porous films from other oxides by using respective metal alkoxides as precursors.

1. Introduction

Porous oxide films find wide use in many different applications, for example as a stationary phase in thin-layer chromatography [1], thermal barrier coatings [2, 3], gas sensors, catalysts and catalyst supports [4, 5] and as active layers in electrochromic devices [6, 7]. Films with desired porous structure and pore- and particle size distribution can either be prepared as having continuous and chemically bonded structure or as consisting of aggregates and agglomerates of oxide nano- and microparticles. The continuous oxide matrix phase can be achieved, for example, by using sol-gel phase separation method, relying on the changing polarities and on the consequent decrease in solubility of hydrolyzing and polymerizing metal- and silicon alkoxides in a solution at the sol-gel transition. Phase separation in the form of spinodal decomposition can be influenced by synthesis parameters like the choice of solvent, solvent concentration, polymer additives, water to alkoxide molar ratio and by the use of alkoxides with nonhydrolyzable organic groups. This enables to achieve wide range of pore sizes and -morphologies in preparation of many different porous oxides [8, 9].

Porous oxide films can also be obtained by assembling nano-and microparticles into porous structures on the conductive substrates by using electrophoretic deposition from the particle suspension to form porous films [10, 11]. For preparation of silica films, one of the common methods for obtaining monodisperse spherical particles is a wet-chemical method pioneered by Stöber and Fink with several later modifications [12, 13]. Sol-gel method has also been combined with emulsion templating, which relies on the oxide formation around the emulsion droplets or deposition of an oxide material at the exterior of emulsion droplets [14, 15, 16]. Mixing of ceramic precursor with salt particles or other selectively leachable phase, followed by compaction by using pressure and consequent leaching yields porous ceramics. Also, the desired pore structure can be achieved in different oxides by the burnout of sufficiently volatile particles or thermally unstable additives [17, 18].

Many of the abovementioned methods of preparing porous oxide layers rely on the availability of suitable oxide particles which are often

* Corresponding author.
E-mail address: martin.timusk@ut.ee (M. Timusk).

https://doi.org/10.1016/j.heliyon.2021.e07675
Received 17 March 2021; Received in revised form 23 May 2021; Accepted 26 July 2021

produced by flame spray pyrolysis. The latter method has many variations but in general requires gas-assisted atomizer to produce aerosol from solvent/oxide precursor mixture, the combustion of which produces a high-temperature flame and results in combustion or decomposition of an oxide precursor. This leads to the formation of oxide nanoparticles in the flame which are collected by filters [19, 20]. The carrier solvent for the oxide precursor may itself either be non-combustible or combustible, having some specific value of heat of combustion and similarly, the carrier gas may either be inert or highly combustible. This process is also commonly used for production of fumed silica.

A classical and well-known method for the preparation of low-density porous silica is the supercritical drying of sol-gel derived alcogels which yields a material called aerogel [21]. Supercritical drying relies on the removal of solvent from the inorganic alcogel pores at supercritical conditions. This enables to avoid the collapse of pore structure and cracking of the sample due to differential capillary pressure that arises from the finite surface tension of the solvent. As the critical temperature and critical pressure are different in case of different solvents, the initial solvent mixture in the gel (water and alcohol) is replaced with a single solvent (typically alcohol, acetone or liquid CO_2) to allow supercritical drying. Supercritical drying of alcogels enables the preparation of aerogels with bulk density in the range of 0.003–0.500 g/cm^3 [22]. Supercritical drying itself does not determine the bulk density of an aerogel. The bulk density is defined by the solid fraction of the alcogel, therefore chosen and determined at the alcogel synthesis stage by the solvent to alkoxide molar ratio. The pre-set value is thus merely fulfilled by the subsequent supercritical drying.

Recently we described a novel method for obtaining aerogel-like low-density micro- and mesoporous silica by combustion of sol-gel derived alcogels in an ambient atmosphere, distinct from previously reported sub- and supercritical drying methods [23]. In the current paper we show that the combustion of sol-gel derived alcogels with specifically chosen composition can yield the release of silica nanoparticles in a simple and controlled manner. The rate of release of nanoparticles and the aggregate size can be set the by the composition of an alcogel. The released silica nanoparticles were directly collected on a substrate to form porous low-density silica films. The deposition was further controlled by applying an electric field between the substrate and the burning alcogel. As such, the process has some resemblance to both electrophoretic deposition and flame-spray pyrolysis, combining aspects from both methods and yields low-density silica with density which is commonly obtained only through supercritical drying of sol-gel derived alcogels. The current paper explores the range of the properties of the deposited silica layers that the presented method enables to achieve in terms of layer morphology, density and composition.

2. Experimental section

2.1. Materials

Tetraethyl orthosilicate (TEOS, 98 %), 1-propanol (>99.5 %), ammonium hydroxide (30–33 % in water) were supplied by Sigma-Aldrich. Tetramethyl orthosilicate (TMOS, 98%) was supplied by Alfa Aesar. All chemicals were used as received.

2.2. Synthesis of silica alcogels

Series of sols were prepared based on TEOS and TMOS as silica precursors by varying TEOS to TMOS molar ratio (0.6:0.4, 0.45:0.55, 0.3:0.7, 0.15:0.85 and 0:1). In case of all of the TEOS/TMOS molar ratios, water to alkoxide molar ratios (R-values) of 2, 3 and 4 was used. 1-propanol was used as a solvent with constant alkoxide to solvent molar ratio of 4 in all of the sols. For alcogel synthesis, NH_4OH (0.04 M in deionized water) was used as a catalyst for hydrolysis and polycondensation reactions. In all synthesized sols 0.04 M NH_4OH solution was added up to R value of 2, followed by addition of pure water in case of samples with R values of 3 and 4. This enabled to achieve equal catalyst concentration in all alcogels, irrespective of final R value. Synthesis of sols was carried out at room temperature (22 °C) in a 100 mL glass beaker by using a magnetic stirrer. All the prepared sols were homogeneous and were mixed for 10 min, followed by filling into hermetically sealed polypropylene containers in 20 mL quantity for gel formation. Gel samples were aged at room temperature for 3–15 days prior to gel combustion and film deposition.

2.3. Deposition of silica films

Low-density silica films were deposited on a stainless steel (Goodfellow, AISI 316), aluminum foil and on the indium tin oxide (ITO)-coated glass slides (Kintec, sheet resistance 15Ω/sq) in an ambient atmosphere by placing a substrate above the burning alcogel. Electrical potential of +7 kV was applied to the substrate with respect to alcogel by using Heinzinger LNC 30000-2pos high voltage source to enhance the collecting of nanoparticles that were released from the burning alcogel (see Figure 1 for the image of the setup). The substrates were cleaned with methanol, acetone and deionized water prior to deposition. The deposition of silica nanoparticles/agglomerates occurs also spontaneously and thus the electric field is not essentially required. Nevertheless, electric field-assisted deposition allows to collect the nanoparticles more efficiently and to achieve more uniform coating.

2.4. Characterization of samples

Scanning electron microscope (SEM) images were acquired with FEI Nova NanoSEM 450. For better conductivity the samples were coated with a thin sub 5 nm layer of gold–palladium alloy prior to SEM imaging by using a Quorum Technologies SC7640 Sputter Coater. Relatively low voltage (5kV) imaging together with stage biasing (4kV), short dwell times (1–2 μs), line and image averaging were used to avoid surface charging artefacts in the images.

In order to evaluate particle/agglomerate size distribution in the films, dynamic light scattering measurements were carried out by using Malvern Zetasizer Nano ZSP. For this purpose, the film material was released from the substrate and transferred into aqueous dispersions by cutting the coated substrates into pieces and placing them into a glass vial filled with water (Milli–Q, pH ~7) and treated with ultrasound probe (Hielscher UP200S) to release the film material from the substrates. The obtained dispersions were stable for many hours without any visible sedimentation, as can be expected at pH ~7 in case of silica.

Fourier-transform infrared spectra of the alcogels were obtained by using Bruker Vertex 70 FT-IR spectrometer with an attenuated total reflection (ATR) accessory.

Mass of the films was measured by weighing the substrates before and after the film deposition. The deposition rate was calculated from the film mass, obtained by the set deposition time. Deposition time of 5–8 min was used in order to obtain sufficient film thickness and weight (typically in the range of 10–45 mg) for reliable measurements. The thickness of the films was measured by imaging the cross-sections of the films by using FEI Nova NanoSEM 450 scanning electron microscope.

Optical transmittance measurements of the porous silica layers were carried out by using a white light source Ocean Optics LS-1, spectrometer Ocean Optics HR2000 + ES and a custom-built optical setup, enabling the measurement of transmittance and optical haze according to the ASTM standard D1003. With this setup, the light that deviates less than 2.5° from the direction of the incident beam after passing the sample is detected as transmitted light. Clean ITO-coated glass slide was used as a reference in the transmittance measurements.

3. Results and discussion

As the experiment relies on the combustion of an alcogel, 1-propanol was chosen as solvent to achieve higher heat of combustion. The heat of

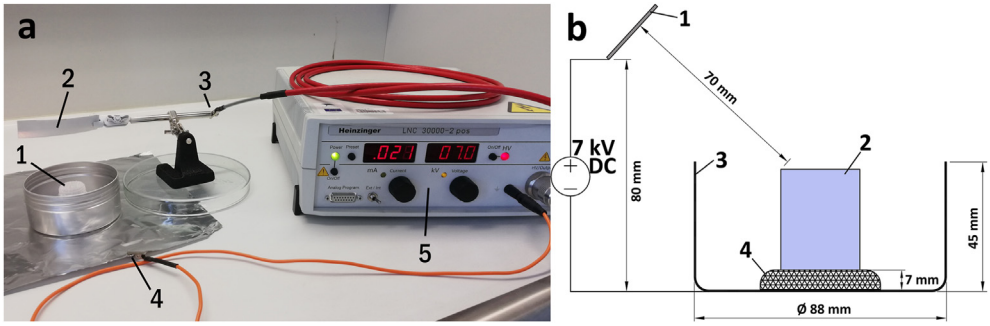

Figure 1. a) Photo of the basic experimental setup for the film deposition from the burning alcogel; 1 – burning alcogel (flame is poorly visible due to high lighting conditions), 2 – stainless steel substrate, 3 – +7 kV connector to the substrate, 4 – electrical ground connector under the burning substrate, 5 – high voltage source. b) Diagram of the experimental setup. 1 – substrate, 2 – alcogel 26.7 mm in diameter and 20 mL in volume, 3 – aluminum cup that contains the burning alcogel, 4 – steel mesh to raise the burning alcogel for a better air flow.

combustion of 1-propanol is ~32 % and ~12% higher compared to methanol and ethanol respectively, resulting in higher flame temperature. Additionally, the use of 1-propanol enables to investigate the hydrolysis reaction of TEOS that results as ethanol as reaction product by using FT-IR spectrometry. If ethanol would be used as a solvent in the synthesis, the additional formation of small amount of ethanol from chemical reactions would not be well discernible from the pre-existing ethanol by using FT-IR spectrometry.

In general, improper choice of solvent in the sol-gel process may induce macroscopic phase separation when it is not desirable but in case of sols similar to those prepared in the current work, no such effect is observable. Additionally, the use of non-parent alcohol may potentially result in alcohol exchange reactions and the formation of mixed alkoxides $Si(OR)_{4-x}$ $(OR')_x$ [24, 25]. Rapid exchange between the methoxy groups of TMOS and the ethoxy groups of the ethanol solvent have been shown to occur [26] and the exchange between the ethoxy groups on TEOS and the propoxy groups of an 1-propanol has been shown [27]. Nevertheless, as the same solvent was used in all of the prepared alcogels, these effects didn't seem to affect the behavior of the system in any relevant manner.

Alcogels prepared by using 60 mol% TEOS required almost 2 days at room temperature to form a gel, irrespective of R-value and at 3 days, the mechanical strength of these gels was barely sufficient to allow handling by fingers. Gels that contained 30 or 15% of TEOS on the other hand both formed a gel in less than 2 h. The gel strength increased notably as TEOS concentration decreased. This indicates incomplete 3D silica skeleton formation, incomplete hydrolysis of TEOS and TEOS acting as a solvent that is diluting the TMOS solution and increasing gel time, rather than contributing to silica skeleton formation and gel strength.

It is common to use both NH_4F and NH_4OH as catalysts in the preparation of TEOS-based sols and alcogels as NH_4OH alone is insufficient for preparation of TEOS-based alcogels whereas for hydrolysis and polycondensation of TMOS, NH_4OH alone is fully sufficient as a catalyst [28, 29, 30]. In general, the rate of hydrolysis of TEOS may be orders of magnitude lower as compared to TMOS, due to steric hindrance of larger alkoxy groups. Therefore, in a sol containing both TEOS and TMOS and only NH_4OH as a catalyst, hydrolysis and homocondensation of TMOS occurs, leaving unreacted or partially reacted TEOS in a solvent phase inside the gel pores.

FT-IR transmittance spectra of the alcogels prepared at the highest TEOS molar concentration (60%) at different R-values (Figure 2) confirm the conclusions described above. Owing to fast hydrolysis, no unreacted TMOS can be expected to be present in the alcogels after 3 days at which alcogel combustion and film deposition took place. FT-IR measurements confirm this to be the case. Absorption peaks characteristic to TMOS at 641, 815 and 1072 cm^{-1} disappear (see Figure 3 for FT-IR transmittance spectra of pure TMOS and TEOS) and although absorption peaks at 1193 and 1464 cm^{-1} have some overlap with 1-propanol absorption peaks, these too seem to have disappeared. This is expected as we have also previously shown TMOS hydrolysis to be complete in a timescale of minutes [31]. TEOS absorption peaks at 787 cm^{-1} with the shoulder at 812 cm^{-1} and a peak at 1168 cm^{-1} are expected to disappear completely at complete hydrolysis of TEOS [32]. These absorption peaks decrease slightly and an intense peak at 958 cm^{-1} disappears completely which corresponds to $\rho(CH_3)$ vibrational mode in TEOS [33]. Also, peak at 1101 cm^{-1} decreases that can be attributed to TEOS.

Low intensity absorption peaks arise at 1455 and 1655 cm^{-1} that can be attributed to the formation of small amount of ethanol. Some other prevalent peaks in ethanol's absorption spectra at 880, 1045 and 1379 cm^{-1} overlap with absorption peaks of alkoxide and 1-propanol and these cannot be clearly observed. Additionally, wide peak near 640 cm^{-1} intensifies which is present in FT-IR spectra of both ethanol and 1-propanol, likely indicating the formation of ethanol. Low intensity ethanol's absorption peak at 1655 cm^{-1} intensifies slightly with increasing R-value, which may indicate slow hydrolysis of TEOS as there is water available in the alcogel, released from polycondensation reaction of silanol groups, originating from TMOS hydrolysis. The peaks at 1054 and 1068 cm^{-1} correspond to 1-propanol, overlapping with intense peak of TEOS at 1072 cm^{-1}. The measured FT-IR spectra of pure TMOS, TEOS and 1-propanol are shown in Figure 3 for comparison. Overall, the measured FT-IR spectra confirm very slow hydrolysis of TEOS, which was also evident by the gel times and by the deterioration of mechanical strength of the alcogels as TEOS concentration was increased.

The photo of the deposited low-density silica films on ITO-coated glass substrates, deposited from alcogels prepared at R = 2 is shown on the inset of Figure 4. The photo of the films deposited on the stainless steel substrates from the alcogels prepared at 3 different R-values is presented on Figure 5. Progressively higher TEOS concentration resulted in increasing deposition rate (also observable visually by the opaque appearance of the films) and thicker films per unit deposition time. The release of nanoparticles was eliminated completely as TEOS concentration was set to 0 mol % (i.e. pure TMOS-based alcogel) or in case of

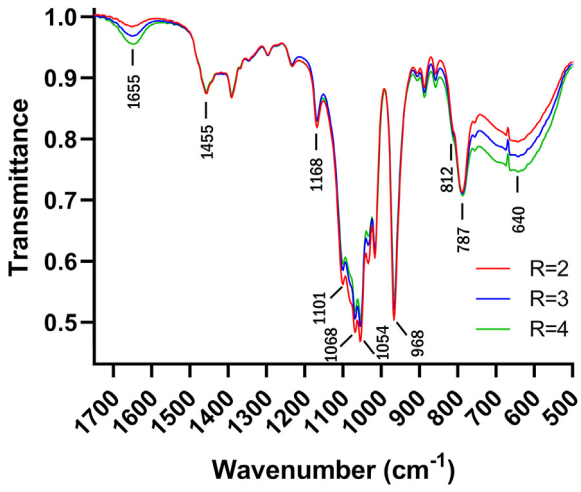

Figure 2. FT-IR spectra of alcogels prepared at different R-values by using 60 mol% of TEOS.

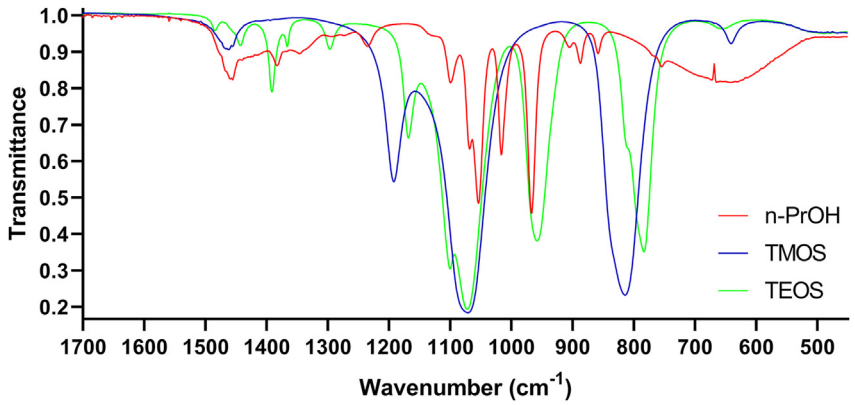

Figure 3. FT-IR spectra of pure precursors for alcogel synthesis - TMOS, TEOS and 1-propanol.

additional catalyst of NH_4F (0.02 M in water) was used, resulting in uncoated substrates in both cases (thus not shown in Figure 4). Therefore, this choice of silica precursors and catalyst enables to achieve gel formation and the preparation of combustible material that exhibits no flow, is easy to handle, burns safely at a convenient rate and exhibits high heat of combustion. At the same time, these alcogels have a composition capable of producing silica nanoparticles from sufficiently volatile, partially hydrolyzed alkoxide monomers and oligomers, evaporated from the burning alcogel pores. TEOS can be expected to decompose in the flame into the silicic acid ($Si(OH)_4$) through complex pathways, followed by the formation of primary particles from gas-phase monomers, surface reactions between particles and gas-phase molecule and cluster–cluster coagulation, leading to particle growth [34, 35].

No light absorption occurs in the films in the visible spectral range, only diffuse reflectance and forward scattering. This gives an opaque appearance to the films. Transmittance below 100% (Figure 4) simply means that some portion of the light that passes through the sample deviates more than 2.5° from the direction of the incident beam and this light is not detected as transmitted light. More scattering occurs in the thicker films, resulting in lower transmittance. Scattering is more intense at the lower end of wavelengths of the visible light since the wavelength of light is comparable to the particle agglomerate- and the pore sizes in the films. For the same reason significantly less scattering occurs in the near-infrared spectral range.

The deposition rate exhibited linear dependence on TEOS concentration and nearly identical behavior at every R-value. For this reason, we further focused on the in-depth analysis only of the films prepared at R = 2. The fact that R-value has no significant influence on the deposition rate further confirms that very little TEOS hydrolysis and incorporation into silica network occurred and the water used in the synthesis can essentially be viewed as being all added to TMOS with effective R-value much larger than the R-value calculated with respect to the sum of both alkoxides in the starting sol. Deposition of the films was carried out 3 and 15 days after the synthesis of alcogels (Figure 6a), allowing to investigate the influence of aging time on the deposition process. The deposition rate decreased by about 27% as the result of the extra 12 days of aging without other noticeable consequences, allowing rather large timeframe for film deposition with nearly identical outcome. The decrease of deposition rate is caused by the slow hydrolysis and polycondensation of TEOS by which the TEOS gets slowly incorporated into non-volatile silica matrix.

By increasing TEOS molar fraction from 15 to 60 mol%, deposition rate increased linearly from 1.397 to 7.119 $\mu g/cm^2*s$ in case of deposition taking place 3 days after the alcogel synthesis and from 1.186 to 5.180 $\mu g/cm^2*s$ in case of alcogels aged for 15 days. The resulting film density was found to be constant at 0.101 ± 0.0086 g/cm^3, irrespective of the deposition rate and TEOS concentration in the alcogel, despite large differences in the coarseness of the films. By assuming the density of skeletal silica particles to equal the value of the density of amorphous silica – 2.195 g/cm^3, the measured bulk density value of the films translates to the porosity value of ~95.4%. The expected value of the density of the skeletal particles is based strongly on the fact that these particles travel through the high-temperature flame before reaching the substrate. The density of the obtained silica films is comparable to silica aerogels prepared by supercritical drying (density in the range of 0.03–0.35 g/cm^3) [36] but with the difference of the deposited films exhibiting different packing of primary particles and the porosity in the form of macropores whereas aerogels prepared by the supercritical drying of inorganic alcogels typically exhibit porosity in the micro- and mesopore range.

The release of silica nanoparticles and consequently the ability to deposit low-density silica films from the burning alcogel was only found to be possible in case of specifically chosen precursors for alcogel synthesis. All of the results clearly show that the release of silica nanoparticles and the possibility of silica film deposition from the burning alcogel results from unreacted or partially reacted TEOS. When synthesis parameters are set such that all of the alkoxide hydrolyses and gets incorporated into 3D silica network, the release of silica nanoparticles ceases.

The exact size of primary particles is somewhat difficult to determine from the SEM images as in order to minimize the charging of the samples,

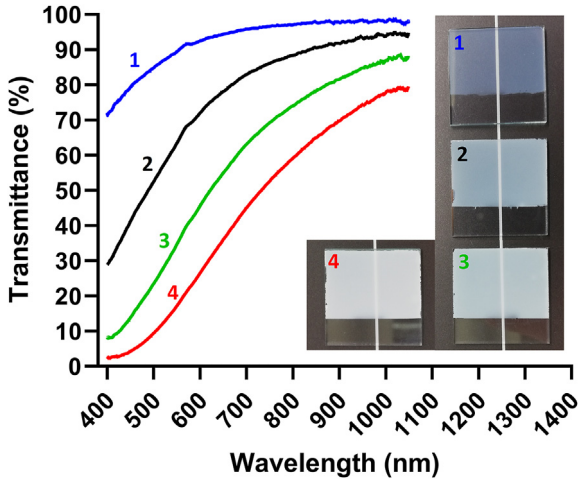

Figure 4. Transmittance spectra of the silica films prepared with equal deposition time of 5 min from alcogels synthesized at R = 2. TEOS concentration in the alcogel with respect to TMOS is 1–15 mol %, 2–30 mol%, 3–45 mol%, and 4–60 mol %. The film thicknesses are 13.2, 26.6, 36.4 and 57.5 μm respectively. An inset shows the photograph of the films on ITO-coated glass substrates. Substrates (25 × 25 mm) are partially uncoated for comparison with the clean substrates.

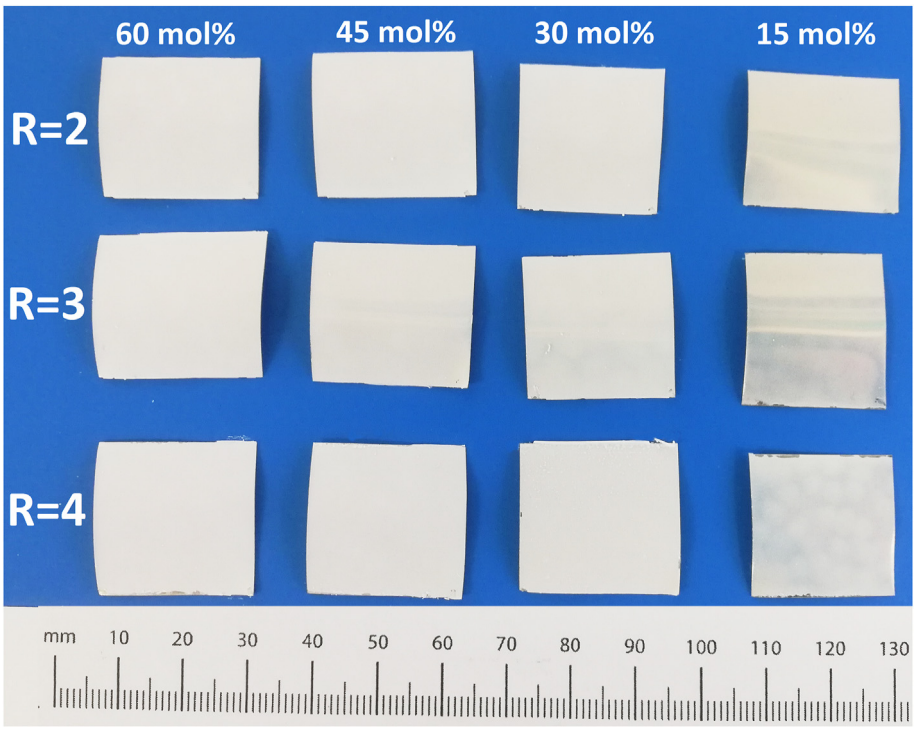

Figure 5. Low-density silica films on stainless steel substrates, prepared by using 60, 45, 30, and 15 mol % of TEOS in the alcogel synthesis with respect to TMOS at R-values of 2, 3 and 4. No film deposition was observed by using 0 mol % of TEOS.

it was necessary to coat the samples with thin layer of metal which itself consists of nanoparticles. Nevertheless, the primary particle size in all of the films can be estimated to be in the range of ~10 nm, irrespective of R-value and the concentration of TEOS in the alcogels. For comparison, primary particle size of 10–75 nm [19] and 7–40 nm [37] has been reported in preparation of silica nanoparticles by flame spray pyrolysis. In the films prepared at R = 2, average aggregate size of primary particles decreased from 79 nm to 32 nm as TEOS concentration decreased from 60 to 15 mol% (Figure 7) with gradually finer structure clearly visible on SEM images. The same trend is visible also in films deposited from alcogels prepared at R = 3 and R = 4 (Figures 8 and 9). At high TEOS concentrations larger secondary particle size is obtained. This is expected as particle concentration during mass transfer is high, leading to high probability of collisions in the flame as the particles travel toward the substrate. At low TEOS concentrations the deposition rate is low and particle agglomerate size is also small as only small amount of collisions are possible during transport due to low concentration.

The cross-sections of the films are shown in Figure 10. Imaging of cross-sections showed that the films are homogeneous throughout the thickness with the same particle size and packing from top to bottom. Some distortion of the film structure and particle compaction is visible at the bottom part of the cross-sections (Figures 10a and 10b). This is due to cutting of the films to expose the cross-section for imaging. The deposited layer thicknesses in Figure 10 are 134, 100, 75 and 37.5 μm, deposited from burning silica alcogels containing 60, 45, 30 and 15 mol % of TEOS from the total alkoxide amount in the alcogels. The deposition time was 7,7,8 and 8 min respectively. The film deposited from the alcogel containing 15 mol% TEOS exhibits bumpy surface on the scale of ~50 μm and slightly inhomogeneous thickness. In other cases, smooth films over large areas could be obtained. The maximum possible layer thickness is in general only limited by the deposition time.

Dynamic light scattering (DLS) measurements of the film material was carried out in order to gain an insight into strength of particle bonding inside the deposited layers. This can't be deduced from SEM imaging, despite discerning primary particles and agglomerates of different sizes. SEM images do not reveal whether particles within the film are strongly or weakly bonded. Samples for DLS measurements were prepared in the form of aqueous dispersions by using the ultrasound

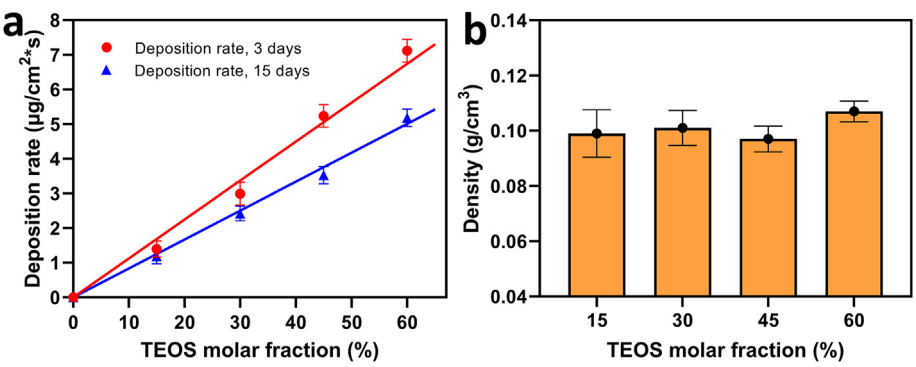

Figure 6. a) Deposition rate by using alcogels prepared at R = 2 and aged for 3 and 15 days before the deposition. b) Deposited silica film density depending on TEOS molar fraction.

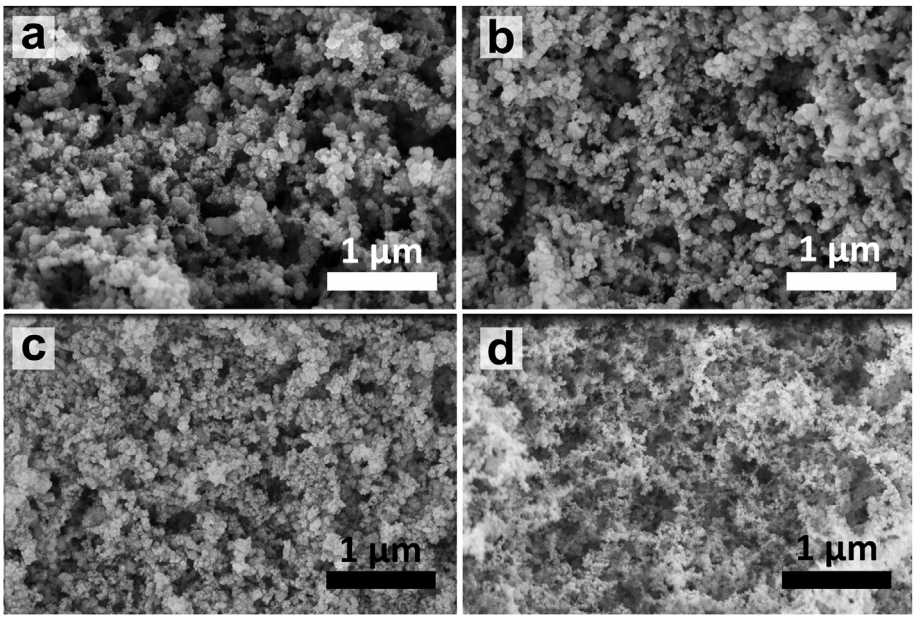

Figure 7. SEM images of silica films deposited from alcogels prepared at R = 2 and at 60 mol% TEOS (a), 45 mol% TEOS (b), 30 mol% TEOS (c) and at 15 mol% TEOS (d).

probe treatment of the coated substrates in water. DLS measurements show z-average diameter of the particles of 290, 254, 241 and 284 nm in samples prepared from alcogels at R = 2 and at 60, 45, 30 and 15 mol% of TEOS respectively (Figure 11a). Main peak distribution analysis showed the average hydrodynamic diameters of 350, 291, 292 and 334 nm and the aggregate size distribution covering the size range of ~0.1–1.3 μm. By comparing the DLS measurement results of all samples prepared at R = 2, 3 and 4, the z-average diameter of the particles was similar and had no correlation with TEOS molar fraction (see also Figures 11b and 11c). This particle size is much larger than the primary particle size and aggregate size visible on SEM images. Ultrasound treatment of samples and the consequent DLS measurements enable to determine the size limit separating the aggregate (chemically strongly bonded particles) and agglomerate (weakly bonded particles) size whereas SEM images only reveal primary particle size and the first noticeable size range of aggregates, formed from the primary particles. The diameters of the commercially available fumed silica primary particles are typically in the range of 5–15 nm which form aggregates of the size of 200–300 nm diameter which in turn bundle into up to micron-size agglomerates [38]. The significant difference between the DLS hydrodynamic particle diameter and the aggregate size on SEM images shows that the agglomeration occurs not only during mass transfer phase prior to the particles reaching the substrate, which determines the aggregate size but also in the films during deposition. The deposited silica films are mechanically weak and can be scraped off the substrates with relatively small effort. This is expected as the films exhibit very low density.

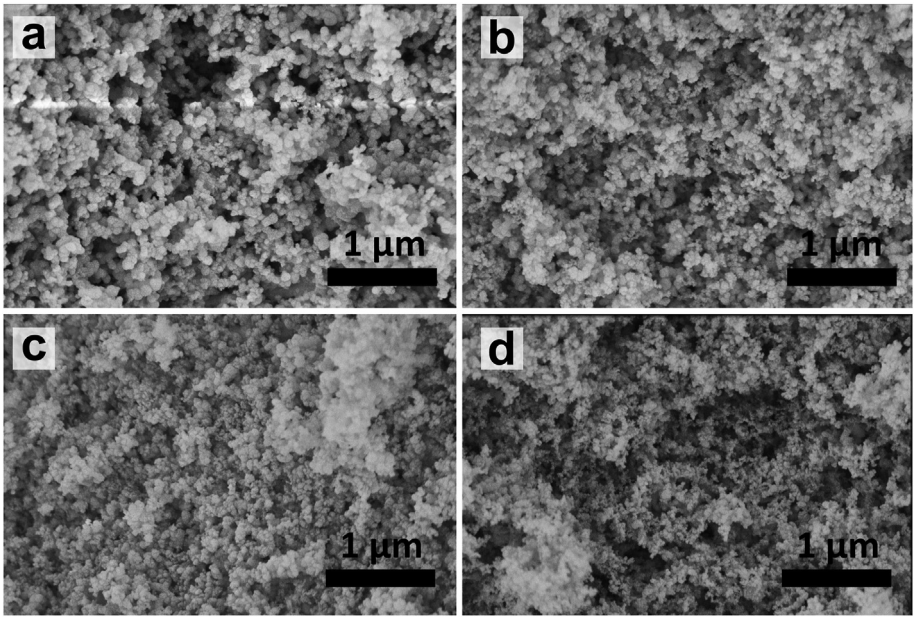

Figure 8. SEM images of silica films deposited from alcogels prepared at R = 3 and at 60 mol% TEOS (a), 45 mol% TEOS (b), 30 mol% TEOS (c) and at 15 mol% TEOS (d).

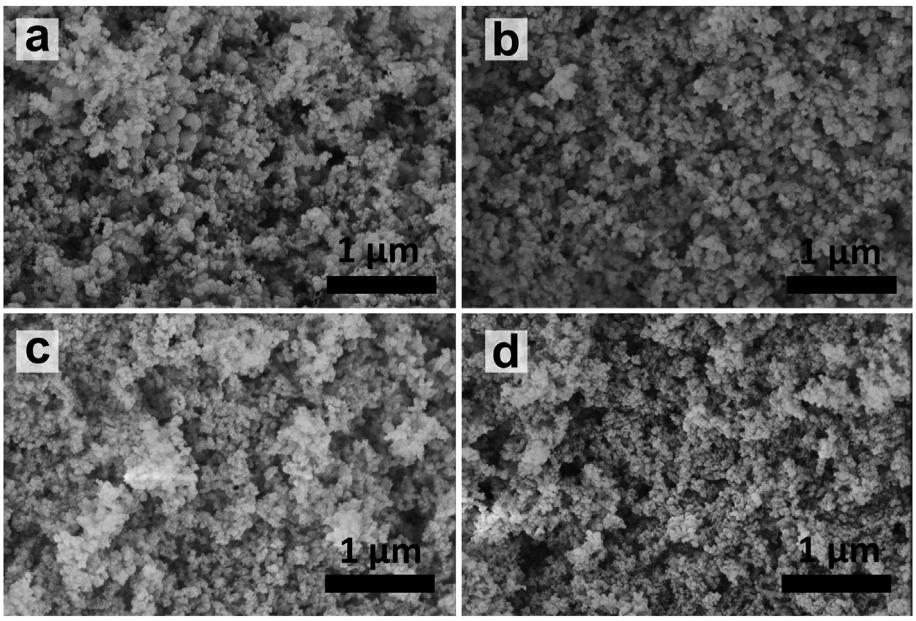

Figure 9. SEM images of silica films deposited from alcogels prepared at R = 4 and at 60 mol% TEOS (a), 45 mol% TEOS (b), 30 mol% TEOS (c) and at 15 mol% TEOS (d).

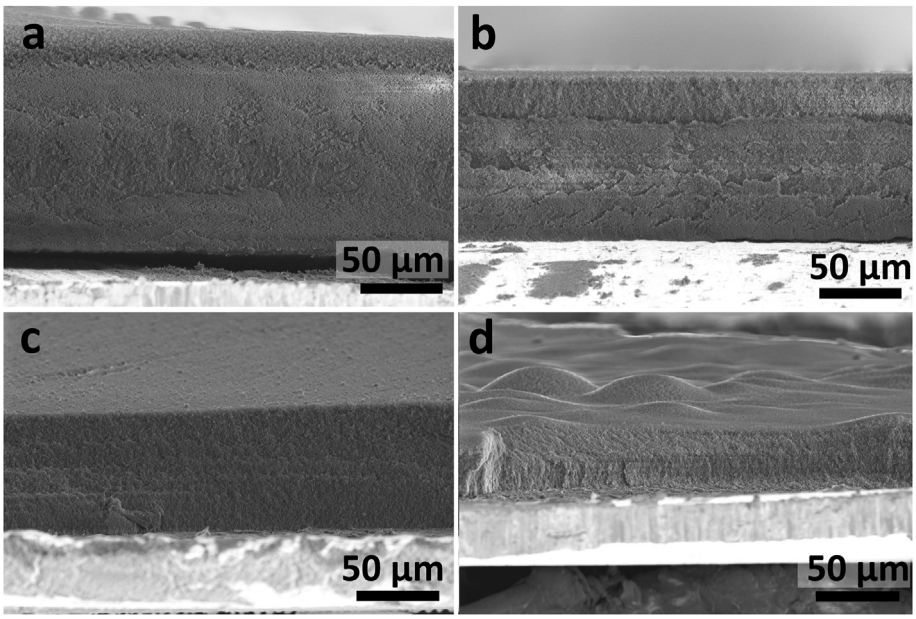

Figure 10. SEM images of the cross-sections of the silica films deposited from alcogels prepared at R = 2 and at 60 mol% TEOS (a), 45 mol% TEOS (b), 30 mol% TEOS (c) and at 15 mol% TEOS (d). The deposition time was 7,7,8 and 8 min and the film thicknesses are 134, 100, 75 and 37.5 μm respectively.

Annealing of the films noticeably increased the strength of the films but the further detailed investigation of this effect remains the focus of the future study.

FT-IR spectra of all of the deposited films are essentially identical (Figure 12) with only the film deposited from alcogel containing 15% of TEOS exhibiting slightly lower overall absorbance due to smaller thickness of the film. The spectra of the deposited films exhibit only 3 absorption peaks – intense peak at 1058 cm^{-1} with a shoulder at 1210 cm^{-1} and lower intensity peaks at 807 and 568 cm^{-1}. These peaks are well known in the FT-IR spectra of silica. A high intensity peak at 1058 cm^{-1} can be attributed to asymmetric stretching of ≡ Si–O–Si ≡. The peak at 807 cm^{-1} corresponds to -Si-O-Si- bending mode and the band at 568 cm^{-1} has been attributed to bending vibrations of O–Si–O [39, 40, 41]. Silanol absorption peaks that are usually observed at around 3750, 3740, 3720, 3657 and 3540 cm^{-1} [42, 43] are completely absent. Also, no alkoxide nor organic residues are detectable Thus, the deposited films consist of pure silica that is silanol-free. The formation of silanol-free silica can be attributed to high-temperatures in the flame exerted to the material during the transport to the substrate. Silanol content has been shown to be one of the major factors affecting the toxicity of the amorphous silica [44]. The damage to the cell membrane from the silica nanoparticles has also been found to depend on the local density of silanol groups, irrespective of crystalline or amorphous nature of the particles [45]. Thus, the silanol-free silica prepared by the method described in the current paper would also be interesting from the viewpoint of particle toxicity studies.

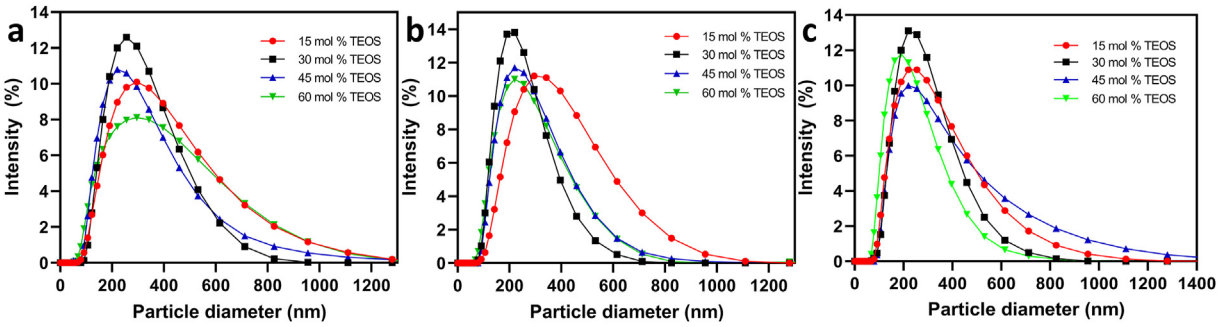

Figure 11. DLS measurement results for the dispersions of film mass deposited from burning alcogels prepared at a) R = 2, b) R = 3 and c) R = 4. The main peak of distribution analysis is shown.

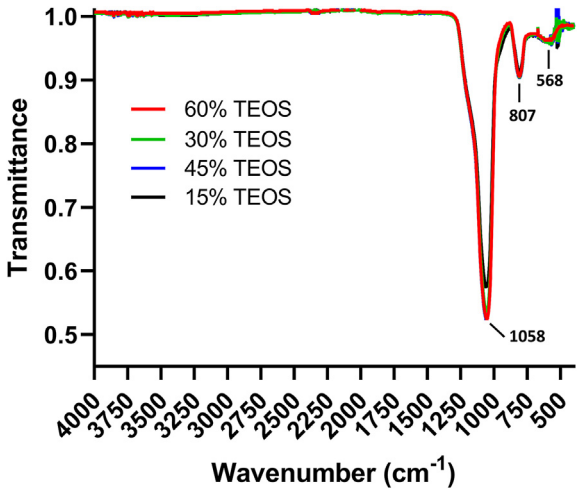

Figure 12. FT-IR spectra of deposited silica films prepared at R = 2 at different concentrations of TEOS.

Sol-gel derived porous silica films have been previously proposed as antireflective coatings [46]. This type of antireflective coating relies on the dependence of the refractive index on the density of the coating whereas the refractive index can be very small in case of low density. The films deposited from the burning alcogels that contain 15% of TEOS from the total amount of alkoxides used, exhibit moderate transparency and low light scattering below the thickness of 30 μm. This can be attributed to very small skeletal particle size and to the fine structure of the films. With further optimization of the deposition process and the decreased pore size in the films, high optical transparency can be expected. That would open up many optical applications of the material with also high optical transmittance in infrared spectral range without absorption caused by the presence of the silanol groups.

4. Conclusions

A new method has been demonstrated for preparation of low-density silica films. The combustion of sol-gel derived silica alcogels in an ambient atmosphere with selected composition and synthesis parameters enables the release of silica nanoparticles (~10 nm) and the deposition of silanol-free silica films in a controlled manner. The density of the obtained films was ~0.101 g/cm^3 and the porosity 95.4%. The described method enables the control of the film morphology and deposition rate simply by the composition of silica alcogel without the need for an aerosol generator or other complex apparatus that is used in flame-spray pyrolysis process. The described method can potentially be extended to the preparation of low-density oxide films from other oxides.

Declarations

Author contribution statement

Martin Timusk: Conceived and designed the experiments; Performed the experiments; Analyzed and interpreted the data; Contributed reagents, materials, analysis tools or data; Wrote the paper.

Triin Kangur, Meeri Visnapuu, Siim Pikker: Performed the experiments.

Andris Šutka, Martin Järvekülg: Contributed reagents, materials, analysis tools or data; Wrote the paper.

Funding statement

This work was supported by Estonian Research Council grant PUT PSG70.

Data availability statement

Data included in article/supplementary material/referenced in article.

Declaration of interests statement

The authors declare no conflict of interest.

Additional information

No additional information is available for this paper.

References

[1] S. Gocan, Stationary phases for thin-layer chromatography, J. Chromatogr. Sci. 40 (2002) 538–549.
[2] J. Medřický, N. Curry, Z. Pala, M. Vilemova, T. Chraska, J. Johansson, N. Markocsan, Optimization of high porosity thermal barrier coatings generated with a porosity former, J. Therm. Spray Technol. 24 (2015) 622–628.
[3] N. Curry, M. Leitner, K. Körner, High-porosity thermal barrier coatings from high-power plasma spray equipment—processing, Perform. Econ. Coating 10 (2020) 957.
[4] G. Frenzer, A. Frantzen, D. Sanders, U. Simon, W.F. Maier, Wet chemical synthesis and screening of thick porous oxide films for resistive gas sensing applications, Sensors 6 (2006) 1568–1586.
[5] G. Frenzer, W.F. Maier, Amorphous porous mixed oxides: sol-gel ways to a highly versatile class of materials and catalysts, Annu. Rev. Mater. Res. 36 (2006) 281–331.
[6] Y. Djaoued, S. Balaji, R. Brüning, Electrochromic devices based on porous tungsten oxide thin films, J. Nanomater. 2012 (2012).
[7] W. Cheng, J. He, K.E. Dettelbach, N.J.J. Johnson, R.S. Sherbo, C.P. Berlinguette, Photodeposited amorphous oxide films for electrochromic windows, Inside Chem. 4 (2018) 821–832.
[8] K. Nakanishi, N. Tanaka, Sol – gel with phase separation: hierarchically porous materials optimized for high-performance liquid chromatography separations, Acc. Chem. Res. 40 (2007) 863–873.
[9] X. Lu, G. Hasegawa, K. Kanamori, K. Nakanishi, Hierarchically porous monoliths prepared via sol–gel process accompanied by spinodal decomposition, J. Sol. Gel Sci. Technol. 95 (2020) 530–550.

[10] K. Hasegawa, H. Nishimori, M. Tatsumisago, T. Minami, Effect of poly (acrylic acid) on the preparation of thick silica films by electrophoretic sol-gel deposition of re-dispersed silica particles, J. Mater. Sci. 33 (1998) 1095–1098.
[11] A. Matsuda, M. Tatsumisago, Handbook of sol-gel science and technology, Handb. Sol-Gel Sci. Technol. (2017).
[12] W. Stöber, A. Fink, E. Bohn, Controlled growth of monodisperse silica spheres in the micron size range, J. Colloid Interface Sci. 26 (1968) 62–69.
[13] H. Nishimori, M. Tatsumisago, T. Minami, Growth mechanism of large monodispersed silica particles prepared from tetraethoxysilane in the presence of sodium dodecyl sulfate, J. Sol. Gel Sci. Technol. 9 (1997) 25–31.
[14] D.J. Pine, A. Imhof, Ordered macroporous materials by emulsion templating, Nature 389 (1997) 948–951.
[15] A. Feinle, M.S. Elsaesser, N. Hüsing, Sol-gel synthesis of monolithic materials with hierarchical porosity, Chem. Soc. Rev. 45 (2016) 3377–3399.
[16] P. Colombo, C. Vakifahmetoglu, S. Costacurta, Fabrication of ceramic components with hierarchical porosity, J. Mater. Sci. 45 (2010) 5425–5455.
[17] C. Galassi, Processing of porous ceramics: piezoelectric materials, J. Eur. Ceram. Soc. 26 (2006) 2951–2958.
[18] A. Inayat, B. Reinhardt, H. Uhlig, W.D. Einicke, D. Enke, Silica monoliths with hierarchical porosity obtained from porous glasses, Chem. Soc. Rev. 42 (2013) 3753–3764.
[19] R. Mueller, L. Mädler, S.E. Pratsinis, Nanoparticle synthesis at high production rates by flame spray pyrolysis, Chem. Eng. Sci. 58 (2003) 1969–1976.
[20] S. Liu, M.M. Mohammadi, M.T. Swihart, Fundamentals and recent applications of catalyst synthesis using flame aerosol technology, Chem. Eng. J. 405 (2021) 126958.
[21] R. Baetens, B.P. Jelle, A. Gustavsen, Review: aerogel insulation for building applications: a state-of-the-art review, Energy Build. 43 (2011) 761–769.
[22] H. Maleki, L. Durães, A. Portugal, An overview on silica aerogels synthesis and different mechanical reinforcing strategies, J. Non-Cryst. Solids 385 (2014) 55–74.
[23] M. Timusk, T. Kangur, J. Locs, A. Šutka, M. Järvekülg, Aerogel-like silica powders by combustion of sol-gel derived alcogels, Microporous Mesoporous Mater. 315 (2021).
[24] J. Livage, Basic principles of sol-gel chemistry, Sol-Gel Technol. Glas. Prod. Users. (2004) 3–14.
[25] R.A. Assink, B.D. Kay, Study of sol-gel chemical reaction kinetics by NMR, Annu. Rev. Mater. Sci. 21 (1991) 491–513.
[26] L.W. Kelts, N.J. Effinger, S.M. Melpolder, Sol-gel chemistry studied by 1H and 29Si nuclear magnetic resonance, J. Non-Cryst. Solids 83 (1986) 353–374.
[27] J.C. Pouxviel, J.P. Boilot, J.C. Beloeil, J.Y. Lallemand, NMR study of the sol/gel polymerization, J. Non-Cryst. Solids 89 (1987) 345–360.
[28] D.B. Mahadik, A.V. Rao, R. Kumar, S.V. Ingale, P.B. Wagh, S.C. Gupta, Reduction of processing time by mechanical shaking of the ambient pressure dried TEOS based silica aerogel granules, J. Porous Mater. 19 (2012) 87–94.
[29] D.J. Suh, T.J. Park, J.H. Sonn, J.C. Lim, Effect of aging on the porous texture of silica aerogels prepared by NH4OH and NH4F catalyzed sol-gel process, J. Mater. Sci. Lett. 18 (1999) 1473–1475.
[30] R.E. Russo, A.J. Hunt, Comparison of ethyl versus methyl sol-gels for silica aerogels using polar nephelometry, J. Non-Cryst. Solids 86 (1986) 219–230.
[31] M. Timusk, A. Kuus, K. Utt, T. Kangur, A. Šutka, M. Järvekülg, M. Knite, Thick silica foam films through combined catalytic decomposition of H 2 O 2 and sol–gel processes, Mater. Des. 111 (2016) 80–87.
[32] F. Rubio, J. Rubio, J.L. Oteo, A FT-IR study of the hydrolysis of Tetraethylorthoselicate (TEOS), Spectrosc. Lett. 31 (1998) 199–219.
[33] M.I. Tejedor-Tejedor, L. Paredes, M.A. Anderson, Evaluation of ATR-FTIR spectroscopy as an "in situ" tool for following the hydrolysis and condensation of alkoxysilanes under rich H2O conditions, Chem. Mater. 10 (1998) 3410–3421.
[34] S. Shekar, M. Sander, R.C. Riehl, A.J. Smith, A. Braumann, M. Kraft, Modelling the flame synthesis of silica nanoparticles from tetraethoxysilane, Chem. Eng. Sci. 70 (2012) 54–66.
[35] M.L. Eggersdorfer, S.E. Pratsinis, Agglomerates and aggregates of nanoparticles made in the gas phase, Adv. Powder Technol. 25 (2014) 71–90.
[36] J.L. Gurav, I.K. Jung, H.H. Park, E.S. Kang, D.Y. Nadargi, Silica aerogel: synthesis and applications, J. Nanomater. 2010 (2010).
[37] L. Mädler, H.K. Kammler, R. Mueller, S.E. Pratsinis, Controlled synthesis of nanostructured particles by flame spray pyrolysis, J. Aerosol Sci. 33 (2002) 369–389.
[38] M.C. Heine, S.E. Pratsinis, High concentration agglomerate dynamics at high temperatures, Langmuir 22 (2006) 10238–10245.
[39] D.L. Wood, E.M. Rabinovich, Study of alkoxide silica gels by infrared spectroscopy, Appl. Spectrosc. 43 (1989) 263–267.
[40] T. López, J.L. Bata-García, D. Esquivel, E. Ortiz-Islas, R. Gonzalez, J. Ascencio, P. Quintana, G. Oskam, F.J. Álvarez-Cervera, F.J. Heredia-López, J.L. Góngora-Alfaro, Treatment of Parkinson's disease: nanostructured sol-gel silica-dopamine reservoirs for controlled drug release in the central nervous system, Int. J. Nanomed. 6 (2011) 19–31.
[41] A. Borba, J.P. Vareda, L. Durães, A. Portugal, P.N. Simões, Spectroscopic characterization of silica aerogels prepared using several precursors-effect on the formation of molecular clusters, New J. Chem. 41 (2017) 6742–6759.
[42] E.A. Paukshtis, M.A. Yaranova, I.S. Batueva, B.S. Bal'zhinimaev, A FTIR study of silanol nests over mesoporous silicate materials, Microporous Mesoporous Mater. 288 (2019) 109582.
[43] P. Šot, C. Copéret, J.A. Van Bokhoven, Fully dehydroxylated silica generated from hydrosilane: surface defects and reactivity, J. Phys. Chem. C (2019).
[44] L. Rubio, G. Pyrgiotakis, J. Beltran-Huarac, Y. Zhang, J. Gaurav, G. Deloid, A. Spyrogianni, K.A. Sarosiek, D. Bello, P. Demokritou, Safer-by-design flame-sprayed silicon dioxide nanoparticles: the role of silanol content on ROS generation, surface activity and cytotoxicity, Part, Fibre Toxicol. 16 (2019) 1–15.
[45] C. Pavan, R. Santalucia, R. Leinardi, M. Fabbiani, Y. Yakoub, F. Uwambayinema, P. Ugliengo, M. Tomatis, G. Martra, F. Turci, D. Lison, B. Fubini, Nearly free surface silanols are the critical molecular moieties that initiate the toxicity of silica particles, Proc. Natl. Acad. Sci. U.S.A. 117 (2020) 27836–27846.
[46] J. Jaglarz, P. Karasinski, E. Skoczek, Optical properties of silica antireflective films formed in sol-gel processes, Phys. Status Solidi Curr. Top. Solid State Phys. 8 (2011) 2645–2648.